Fractal dimensions and two-dimensional slow-fast systems

Peer-reviewed author version

HUZAK, Renato; CRNKOVIC, Vlatko & Vlah, Domagoj (2021) Fractal dimensions and two-dimensional slow-fast systems. In: JOURNAL OF MATHEMATICAL ANALYSIS AND APPLICATIONS, 501 (2) (Art N° 125212).

DOI: https://doi.org/10.1016/j.jmaa.2021.125212
Handle: http://hdl.handle.net/1942/33877

Fractal dimensions and two-dimensional slow-fast systems

Renato Huzak*

Hasselt University, Campus Diepenbeek, Agoralaan Gebouw D, 3590 Diepenbeek, Belgium

Vlatko Crnković, Domagoj Vlah

University of Zagreb, Faculty of Electrical Engineering and Computing, Department of Applied Mathematics, Unska 3, 10000 Zagreb, Croatia

Abstract

In our paper we present a fractal analysis of canard cycles and slow-fast Hopf points in 2-dimensional singular perturbation problems under very general conditions. Our focus is on the orientable case (e.g. $\mathbb{R}^2$) and the non-orientable case (e.g. the Möbius band). Given a slow-fast system, we generate a sequence of real numbers using the so-called slow relation function and compute a fractal dimension of that sequence. Then the value of the fractal dimension enables us to determine the cyclicity and bifurcations of canard cycles in the slow-fast system. We compute the fractal dimension of a slow-fast Hopf point depending on its codimension. Our focus is on the *box dimension, one-sided dimensions and the fractal zeta-function*. We also find explicit fractal formulas of Cahen-type for the computation of the above fractal dimensions and use them to detect numerically the number of canard limit cycles.

Keywords: slow-fast systems, slow relation function, box dimension, fractal zeta function, slow-fast Hopf point

1 Introduction

A typical problem in the study of fractal properties of dynamical systems involves finding whether a sequence of real numbers $\{x_0, x_1, \dots\}$ is generated by a deterministic system or a random process (see e.g. the so-called Grassberger-Procaccia algorithm [14, 15] and the notion of correlation dimension). Following Takens [31] relevant information about deterministic dynamical systems

*Corresponding author
Email address: renato.huzak@uhasselt.be

(entropy, dimensions of attractors, etc.) can be obtained from time series generated by the systems without knowing the equations of motion. In [11, 36] it has been shown that fractal analysis (box dimension, Minkowski content, etc.) of the spiral trajectories around a focus or a limit cycle in planar systems can be used to find the number of limit cycles born after perturbation near the focus or the limit cycle. *In our paper, we propose a new approach to the fractal analysis of sequences that can be used to reconstruct the number of limit cycles and the type of bifurcations in families of 2-dimensional slow-fast systems, given a sequence of real numbers generated by the system.* Thus, our starting point is a smooth family of slow-fast vector fields

$$X_{\epsilon,\lambda} : \begin{cases} \dot{x} &= f(x, y, \epsilon, \lambda) \\ \dot{y} &= \epsilon g(x, y, \epsilon, \lambda), \end{cases} \tag{1}$$

where $\epsilon \geq 0$ is the singular parameter kept small, $\lambda \sim \lambda_0 \in \mathbb{R}^m$ and f, g are smooth functions (in our paper "smooth" is C^∞-smooth). When $\epsilon = 0$, we suppose that (1) has a curve of singularities $\{f(x, y, 0, \lambda) = 0\}$ for all $\lambda \sim \lambda_0$ and (fast) regular orbits. The curve is called the critical or slow curve (see Figure 1). The critical curve contains normally attracting parts, normally repelling parts and contact points between them. At the contact points both eigenvalues are equal to zero. It should be clear that the so-called fast subsystem $X_{0,\lambda}$ describes the dynamics of $X_{\epsilon,\lambda}$ when $\epsilon > 0$ and $\epsilon \sim 0$, away from the critical curve. Near the critical curve, away from the contact points, the dynamics of $X_{\epsilon,\lambda}$ can be studied by using the so-called slow dynamics $y' = g(x, y, 0, \lambda)$. Since $\frac{\partial f}{\partial x} \neq 0$ at normally hyperbolic singularities, the slow dynamics can be written as $y' = \tilde{g}(y, \lambda)$ where $\tilde{g}$ is smooth (we can get rid of x in g by applying the Implicit Function Theorem to $\{f = 0\}$). Since the contact points are nilpotent or more degenerate, one uses a family blow-up to desingularize them (for more details see e.g. [9, 21]).

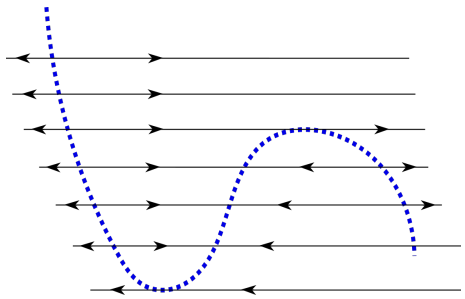

Figure 1: The fast subsystem of $X_{\epsilon,\lambda}$.

For $\epsilon = 0$, we typically deal with slow-fast cycles, i.e. limit periodic sets consisting of fast regular orbits and parts of the slow curve. They can produce limit cycles in $X_{\epsilon,\lambda}$. A slow-fast cycle is called a *canard* cycle if it contains both attracting and repelling parts of the slow curve. *In this paper our focus is on the study of limit cycles Hausdorff close to canard cycles using fractal dimensions.* It is well known that the cyclicity of the canard cycles can be found by studying zeros of a so-called slow divergence integral (see [9, 3]). The slow divergence integral essentially consists of components of the form $I = \int_p^0 \frac{\operatorname{div} X_{0,\lambda} dy}{\tilde{g}(y,\lambda)}$ computed

along the attracting (resp. repelling) part if p is a normally attracting (resp. repelling) singularity (0 represents the contact point). For more details see later sections. One of the reasons why we focus on the fractal approach is that the slow divergence integral can easily be computed only in some special cases (see e.g. [5, 8, 9, 26, 35]). Our method consists of a (numerical) computation of the fractal dimension of one convergent sequence (hence there is no need to compute the multiplicity of zeros of the slow divergence integral).

In the slow-fast setting, we distinguish between two different families of fractal dimensions computed for a sequence of real numbers. In the first family, we deal with the fractal dimensions that are trivial and therefore not suitable for the study of limit cycles in singular perturbation problems. For example, the Hausdorff dimension and the packing dimension are zero due to their countable stability property (see [12]). The correlation dimension will also be zero (for more details see Section 2). The second family contains fractal dimensions that are nontrivial and this will give a "one-to-one correspondence" between their values and the number of limit cycles (*the box dimension, the one-sided or lateral dimension, a geometric (or fractal) zeta-function*). The box dimension measures the density of the sequence (see [12, 33] or Section 2). The bigger the box dimension of the sequence, the higher the density of the sequence and more limit cycles can be born in slow-fast systems. This has been observed in [18, 20] where a so-called *box dimension method* for the computation of the number of limit cycles Hausdorff close to *balanced canard cycles with one or two breaking parameters* has been developed (for more details see Section 3).

The goal of our paper is twofold. We generalize the box dimension method to balanced 1– and 2–canard cycles defined on a *Möbius band*. For example, if the box dimension of one orbit of a slow relation function is zero, then there exists a *period-doubling bifurcation* near the 1–canard cycle. The slow relation function assigns to every point p_+ on the repelling part of the critical curve the point p_- on the attracting part of the critical curve such that the slow divergence integral along $[p_-, p_+]$ is equal to zero. This definition is motivated by the so-called entry-exit relation (see e.g. [1] and later sections). One of the main advantages of our box-dimension method is that we don't have to work directly with the Poincaré map attached to the 1–canard cycle to prove the existence of the period doubling bifurcation. In the slow-fast setting the Poincaré map contains $\exp(I/\epsilon)$-terms that are difficult to analyze from a numerical point of view (see [4, 2]). We replace the fractal analysis of the Poincaré map with the fractal analysis of one orbit of the slow relation function. The box dimension of orbits of the Poincaré map in the presence of the period doubling bifurcation is $\frac{2}{3}$ (see [11]). We also introduce two new fractal methods for the detection of the cyclicity and bifurcations of balanced canard cycles in the orientable case and the nonorientable case, namely the *one-sided dimension method* and the *fractal zeta-function method*. We refer to [12, 33, 34] or Section 2 for a definition of the one-sided dimension (sometimes called the lateral dimension or the interior box dimension). Roughly speaking, the one-sided dimension measures a fractal complexity of $\{x_0, x_1, \dots\}$ relative to a bounded open set $U \subset \mathbb{R}$ with $\{x_0, x_1, \dots\} \subset \partial U$. A definition of fractal-zeta functions and fractal strings can be found in e.g. [24, 25] (see also Section 2). In our slow-fast setting, the fractal zeta-function will be associated to a fractal string defined using the slow relation function. *We prove that the abscissa of convergence*

of the fractal-zeta function tells us how many limit cycles can be born from balanced canard cycles. We also extend the slow relation function to a slow-fast Hopf point and prove a bijective correspondence between the codimension of the slow-fast Hopf point and the box dimension of one orbit generated by the slow relation function. We point out that the same has been done in [17, 36] for the regular Hopf case but using orbits generated by the Poincaré map defined near a focus. (In our slow-fast setting it is easier to compute orbits of the slow relation function and we don't need to introduce the family blow-up to prove our results.)

Second, we find three simple formulas that can be used to calculate the box dimension and the one-sided dimension of a (decreasing and bounded) sequence $\{x_0, x_1, ...\}$, generated by slow-fast systems (see Theorem 1). We compare their speed of convergence while varying the multiplicity and the nonzero coefficient of the slow-relation function (see Section 7). Then we apply them to find 4 (canard) limit cycles in a classical Liénard equation of degree 6 (see Section 7.3). More precisely, we take the classical Liénard equation (15) of degree 6 studied in [4] and detect numerically 3 convergent orbits (with different limits), generated by the slow relation function, each having the box dimension equal to 0. This corresponds to 3 simple zeros of the slow divergence integral of (15). Let us recall that the existence of the 3 simple zeros has been proved in [4] working directly with the slow divergence integral (this implies the existence of 4 limit cycles). Here, we use a pure fractal approach. As explained in [4], the existence of a classical Liénard equation of degree 6 with 4 limit cycles is a counterexample to the conjecture of Lins, de Melo and Pugh formulated in 1976 with at most $[\frac{n-1}{2}]$ limit cycles in classical Liénard equations of degree n ($[\cdot]$ denotes "the greatest integer equal or below"). Thus, the box dimension method can be useful to explore the coefficient space of (polynomial) vector fields to find lower bounds for the number of limit cycles.

The reason why we deal with smooth families of planar slow-fast systems is because the smooth setting allows us to use the slow divergence integral in the proof of the results stated in Sections 3–5. It would be interesting to generalize the results to (linear or nonlinear) piecewise-smooth systems where canards, quasi-canards, duck traps, non-smooth saddle-nodes, super-explosions, etc. can be observed (see e.g. [6, 22, 23, 27, 29, 30] and references therein).

In Section 2 we study the fractal zeta-function, the box dimension and the one-sided dimension of convergent sequences generated by one-dimensional discrete dynamical systems (see Theorems 1 and 2). In Section 3 we define a planar slow-fast model with a Hopf breaking mechanism, and state our main results. In Section 4 we focus on the Möbius band and state the main results. Section 5 is devoted to the fractal analysis of slow-fast Hopf point. We prove the main results in Section 6. As already mentioned, Section 7 is devoted to applications.

2 Fractal dimensions and geometric zeta function

2.1 The box dimension and one-sided dimensions

Let's first define the notion of box dimension and of one-sided dimension for bounded sets in one-dimensional ambient space $\mathbb{R}$ (similar definitions can be

used in higher-dimensional Euclidean spaces). Let $\delta > 0$ and $\delta \sim 0$. We denote by $U(\delta)$ the δ-neighborhood (sometimes called the Minkowski sausage) of a bounded set U. Thus $U(\delta)$ is the set of all points with a distance from $U \leq \delta$. If $|U(\delta)|$ is the Lebesgue measure of $U(\delta)$, then the lower box dimension of U (resp. the upper box dimension of U) is given by

$$\underline{\dim}_B U = \liminf_{\delta \to 0} \Big(1 - \frac{\ln |U(\delta)|}{\ln \delta}\Big) \Big(\text{resp. } \overline{\dim}_B U = \limsup_{\delta \to 0} \Big(1 - \frac{\ln |U(\delta)|}{\ln \delta}\Big)\Big).$$

If $\underline{\dim}_B U$ and $\overline{\dim}_B U$ are equal, then we denote the common value by $\dim_B U$ and call it the box dimension of U. We refer to [12] for other equivalent definitions of the box dimension.

Suppose now that U is a bounded open set (in $\mathbb{R}$) such that $|\partial U| = 0$ (∂U denotes the boundary of U). If U_0 is contained in ∂U, then we define interior box dimensions of U_0 by

$$\underline{\Delta}_{int}(U_0) = \liminf_{\delta \to 0} \Big(1 - \frac{\ln |U_0(\delta) \cap U|}{\ln \delta}\Big),\ \overline{\Delta}_{int}(U_0) = \limsup_{\delta \to 0} \Big(1 - \frac{\ln |U_0(\delta) \cap U|}{\ln \delta}\Big).$$

If $\underline{\Delta}_{int}(U_0) = \overline{\Delta}_{int}(U_0)$, then we denote it by $\Delta_{int}(U_0)$. Similarly, we define exterior box dimensions of U_0 (we replace $\underline{\Delta}_{int}(U_0)$, $\overline{\Delta}_{int}(U_0)$, $\Delta_{int}(U_0)$ and U with $\underline{\Delta}_{ext}(U_0)$, $\overline{\Delta}_{ext}(U_0)$, $\Delta_{ext}(U_0)$ and $\mathbb{R} \setminus \overline{U}$ in the above definition). For all $U_0 \subset \partial U$, we have $\overline{\dim}_B U_0 = \max\{\overline{\Delta}_{int}(U_0), \overline{\Delta}_{ext}(U_0)\}$ (see e.g. [34]).

Our goal is to compute the box dimension and the one-sided box dimensions of any orbit of a smooth function G accumulating at a fixed point of G. More precisely, we define $G(x) := x - F(x)$ where F is smooth and nondecreasing on $[0, \rho[$ (for some small $\rho > 0$), $F(0) = 0$ and $0 < F(x) < x$ for all $x \in]0, \rho[$. Let $x_0 \in]0, \rho[$ be arbitrary but fixed, then we denote by U_0 the orbit of x_0 by G, i.e. $U_0 = \{x_n = G^n(x_0) | n \in \mathbb{N}\}$. The orbit tends monotonically to zero. We say that the multiplicity of the fixed point 0 of G is l if $x = 0$ is a zero of multiplicity l of F (i.e. $F(0) = \cdots = F^{(l-1)}(0) = 0$ and $F^{(l)}(0) \neq 0$).When $F^{(l)}(0) = 0$ for all $l \in \mathbb{N}$, then the multiplicity of the fixed point 0 of G is ∞.

If $F_1(\delta)$ and $F_2(\delta)$ are two positive functions with $\delta \sim 0$ and $\delta > 0$, then we write $F_1(\delta) \simeq F_2(\delta)$ as $\delta \to 0$ if there exist two positive constants C and D such that $CF_2(\delta) \leq F_1(\delta) \leq DF_2(\delta)$ for all $\delta \sim 0$ and $\delta > 0$. We use a similar definition for sequences as $n \to \infty$.

Theorem 1. *Let $F : [0, \rho[\to \mathbb{R}$ be a smooth nondecreasing function, $F(0) = 0$ and $0 < F(x) < x$ for all $x \in]0, \rho[$. Let $U_0 = \{x_0, x_1, \dots\}$ be the orbit of x_0 by G, with $G = id - F$ and $x_0 \in]0, \rho[$. Then the following statements are true:*

1. *There is a one-to-one correspondence between the multiplicity l of the fixed point 0 of G and the box dimension of U_0 (or the interior box dimension of U_0 relative to a bounded open set $U := \cup_{n=0}^{\infty}]x_{n+1}, x_n[$) given by*

$$\dim_B U_0 = \Delta_{int}(U_0) = \frac{l-1}{l},\ l \in \{1, 2, \dots\} \cup \{\infty\}$$

with $\frac{\infty}{\infty} := 1$. Moreover, we have $\Delta_{ext}(U_0) = 0$ relative to $\mathbb{R} \setminus \overline{U}$. As a simple consequence of these results, the box dimension, the interior box dimension and the exterior box dimension of U_0 are independent of the initial point x_0.

2. *When the multiplicity $l \in \{1, 2, \dots\}$, we have:*

$$l = \frac{1}{1 - \lim_{n\to\infty} \left(\frac{\ln n}{-\ln(x_n - x_{n+1})} \right)}. \tag{2}$$

This is also true for $l = \infty$ if we replace "$\lim$" by "$\limsup$" in (2).

3. *When the multiplicity $l \in \{1, 2, \dots\}$, we have:*

$$l = \frac{1}{1 - \lim_{n\to\infty} \left(\frac{1}{1 - \frac{\ln x_n}{\ln n}} \right)}. \tag{3}$$

This is also true for $l = \infty$ if we replace "$\lim$" by "$\limsup$" in (3).

4. *When the multiplicity $l \in \{1, 2, \dots\} \cup \{\infty\}$, we get:*

$$l = \frac{1}{1 - \lim_{n\to\infty} \left(1 - \frac{\ln\left(n(x_n - x_{n+1}) + x_n\right)}{\ln\left(\frac{x_n - x_{n+1}}{2}\right)} \right)}. \tag{4}$$

Proof. Statement 1. Following [11] or [28], we know that the box dimension of U_0 exists and the following bijective correspondence holds: $l = \frac{1}{1-\dim_B U_0}$ for $l = 1, 2, \dots$ and $\dim_B U_0 = 1$ for $l = \infty$. We prove the same for $\Delta_{int}(U_0)$. It is clear that $|U_0(\delta) \cap U| = |U_0(\delta)| - 2\delta$ for $\delta \sim 0$ and $\delta > 0$. This implies that for a small $\delta > 0$ $|U_0(\delta) \cap U|$ is the Lebesgue measure of the δ-neighborhood of $U_0 \setminus \{x_0\}$, i.e. of the orbit of x_1 by G. Following Theorem 1 in [28], the box dimension of G is independent of the initial point, i.e. $\dim_B U_0 = \dim_B(U_0 \setminus \{x_0\})$. Thus, $\dim_B U_0 = \Delta_{int}(U_0)$. Since $\mathbb{R} \setminus \overline{U} =]-\infty, 0[\cup]x_0, \infty[$, it follows that $|U_0(\delta) \cap (\mathbb{R} \setminus \overline{U})| = 2\delta$ and thus $\Delta_{ext}(U_0) = 0$.
Statement 2. First, let's suppose that $1 < l < \infty$. Then $x_n \simeq n^{-\frac{1}{l-1}}$ as $n \to \infty$ (see Theorem 1 in [11]). This implies that $x_n - x_{n+1} = f(x_n) \simeq n^{-\frac{l}{l-1}}$ and therefore $\lim_{n\to\infty} \frac{\ln n}{-\ln(x_n - x_{n+1})} = \frac{l-1}{l}$. This implies the result. When $l = 1$, then it is not difficult to see that $G(x) \leq \alpha x$ with $\alpha \in]0, 1[$ (resp. $G(x) \leq Mx^\beta$ for some $\beta > 1$ and $M > 0$) if $F'(0) < 1$ (resp. $F'(0) = 1$). From this it follows that $x_n \leq \alpha^n x_0$ (resp. $x_n \leq M^{\frac{\beta^n - 1}{\beta - 1}} x_0^{\beta^n}$). Now we have $x_n - x_{n+1} = F(x_n) < x_n \leq \alpha^n x_0$ (resp. $\leq M^{\frac{\beta^n - 1}{\beta - 1}} x_0^{\beta^n}$) and

$$0 \leq \frac{\ln n}{-\ln(x_n - x_{n+1})} \leq \frac{\ln n}{-\ln x_0 - n \ln \alpha} \left(\text{resp. } \leq \frac{\ln n}{\ln M^{\frac{1}{\beta-1}} - \beta^n \ln(M^{\frac{1}{\beta-1}} x_0)} \right).$$

The above sequences tend to zero as $n \to \infty$ ($M^{\frac{1}{\beta-1}} x_0 < 1$ for x_0 positive and small). This implies (2). When $l = \infty$, then the result for $\limsup$ follows directly from Theorem 2.1.33 in [24] or from Section 3.4 in [33].
Statement 3. When $1 \leq l < \infty$, the proof of Statement 3 is similar to the proof of Statement 2. When $l = \infty$, we use Section 3.4 in [33] (the Borel rarefaction index of U_0 is equal to the upper box dimension).
Statement 4. Since the sequence $(\delta_n)_{n=1}^\infty := (\frac{x_n - x_{n+1}}{2})_{n=0}^\infty$ tends monotonically to zero, Statement 1 and the definition of the box dimension imply that

$$\dim_B U_0 = \dim_B(U_0 \setminus \{x_0\}) = \lim_{n\to\infty} \left(1 - \frac{\ln |(U_0 \setminus \{x_0\})(\delta_n)|}{\ln \delta_n} \right).$$

The decomposition of $(U_0 \setminus \{x_0\})(\delta_n)$ into tail and nucleus (see e.g. [33]) gives us the following expression:

$$\begin{aligned} |(U_0 \setminus \{x_0\})(\delta_n)| &= 2\delta_n n + (x_{n+1} + 2\delta_n) \\ &= n(x_n - x_{n+1}) + x_n. \end{aligned}$$

This, together with Statement 1, implies (4). □

Remark 1. *From numerical experiments we believe that (2) is also true when $l = \infty$. In other words, we expect* $\liminf_{n\to\infty} \frac{\ln n}{-\ln(x_n - x_{n+1})} = 1$ *to hold in case $l = \infty$. The same is true for (3).*

Remark 2. *In the proof of Theorem 1 we often use Theorem 1 from [11] if $l \in \{2, 3, \dots\}$. Here we point out that Theorem 1 from [11] is proved for a more general F: if $F(x) \simeq x^\alpha$, as $x \to 0$, with a real number $\alpha > 1$, then $x_n \simeq n^{-\frac{1}{\alpha-1}}$ as $n \to \infty$ and $\dim_B U_0 = \frac{\alpha-1}{\alpha}$. We use this general form in Section 5.*

2.2 Geometric zeta-functions

The set U defined in Theorem 1 is often called the *canonical geometric realization* of the *fractal string* $(x_n - x_{n+1})_{n=0}^\infty$ (see [24]). More precisely, a nonincreasing sequence $\mathcal{S} = (s_n)_{n=0}^\infty$ of positive numbers such that $\sum_{n=0}^\infty s_n$ is convergent is called a fractal string. We define a zeta function associated with the fractal string $\mathcal{S}$:

$$\zeta_{\mathcal{S}}(z) := \sum_{n=0}^{\infty} s_n^z$$

for all $z \in \mathbb{C}$ such that $\mathrm{Re}(z) > D(\zeta_{\mathcal{S}}) := \inf\{x \in \mathbb{R} \mid \sum_{n=0}^\infty s_n^x < \infty\}$. The function $\zeta_{\mathcal{S}}$ (resp. $D(\zeta_{\mathcal{S}})$) is called the *geometric zeta-function* of $\mathcal{S}$ (resp. the *abscissa of convergence* of $\zeta_{\mathcal{S}}$). We can assume that the infimum in the definition of $D(\zeta_{\mathcal{S}})$ is taken over $x \in [0, 1]$ (see [24]). A *geometric realization* of $\mathcal{S}$ is any disjoint union $\cup_{n=0}^\infty I_n$ of bounded open intervals such that s_n is the length of I_n.

The following result gives a bijective correspondence between the abscissa of convergence of the zeta-function of $\mathcal{S} = (x_n - x_{n+1})_{n=0}^\infty$ and the multiplicity of the fixed point 0 of G. We use Theorem 1.

Theorem 2. *Suppose that a (C^∞-) smooth function F satisfies the conditions of Theorem 1. Let $U_0 = \{x_0, x_1, \dots\}$ be the orbit of x_0 by $G = id - F$ and let $U = \cup_{n=0}^\infty]x_{n+1}, x_n[$ be a geometric realization of the fractal string $\mathcal{S} = (x_n - x_{n+1})_{n=0}^\infty$. Then the following statements are true.*

1. *We have $\dim_B U_0 = \Delta_{int}(U_0) = D(\zeta_{\mathcal{S}})$ where $D(\zeta_{\mathcal{S}})$ is the abscissa of convergence of $\zeta_{\mathcal{S}}$.*

2. *There is a one-to-one correspondence between the multiplicity l of the fixed point 0 of G and the abscissa of convergence $D(\zeta_{\mathcal{S}})$ given by*

$$l = \frac{1}{1 - D(\zeta_{\mathcal{S}})}.$$

($l = \infty$ when $D(\zeta_{\mathcal{S}}) = 1$.) As a simple consequence of this result, the abscissa of convergence $D(\zeta_{\mathcal{S}})$ is independent of the initial point $x_0 \in]0, \rho[$.

Proof. First, note that the fractal string $\mathcal{S}$ is well defined because $\mathcal{S} = (F(x_n))_{n=0}^{\infty}$ is a (strictly) decreasing sequence of positive numbers and $\sum_{n=0}^{\infty}(x_n - x_{n+1}) = x_0 < \infty$. Following Theorem 2.1.55 and Corollary 2.1.57 in [24], we get $\overline{\dim}_B U_0 = \overline{\Delta}_{int}(\partial U) = D(\zeta_{\mathcal{S}})$. Since $\dim_B U_0$ and $\Delta_{int}(U_0)$ exist (see Theorem 1.1), Statement 1 is proved. Statement 2 follows directly from Statement 1 and Theorem 1.1. □

Remark 3. *The set $\{Re z > \dim_B U_0\}$ is the biggest right open half-plane where $\zeta_{\mathcal{S}}$ can be holomorphically continued. Moreover, $\zeta_{\mathcal{S}}(z)$ tends to $+\infty$ as $z \to (\dim_B U_0)^+$ and $z \in \mathbb{R}$. For more details see [25] or [24].*

Example 2.1. Consider $U_0 = \{1, \frac{1}{2}, \frac{1}{3}, \dots\}$. Then $\dim_B U_0 = 0.5$ (see e.g. [12]) and this is the abscissa of convergence of $\zeta_{\mathcal{S}}(z) = \sum_{n=1}^{\infty} \frac{1}{n^z(n+1)^z}$. It can be easily seen that the orbit U_0 is generated by $G(x) = x - \frac{x^2}{1+x}$. Thus, the multiplicity of G at $x = 0$ is 2.

2.3 The correlation integral and correlation dimension

The correlation dimension of a sequence $\{x_0, x_1, \dots\}$ of real numbers is a double limit $\lim_{\delta \to 0}\left(\lim_{n\to\infty} \frac{\ln C(n,\delta)}{\ln \delta}\right)$ where $C(n, \delta)$ is the so-called (sample) correlation integral given by

$$C(n, \delta) = \frac{p}{\binom{n}{2}}$$

where p is the number of distinct pairs (x_i, x_j), $0 \le i < j \le n-1$, with the property that $|x_i - x_j| \le \delta$. We assume that the double limit exists (for more details about this definition see e.g. [32]). If the sequence is generated by a function G defined in Section 2.1, then its correlation dimension is trivial.

Proposition 1. *Suppose that a (C^∞-) smooth function F satisfies the conditions of Theorem 1. Let $U_0 = \{x_0, x_1, \dots\}$ be the orbit of x_0 by $G = id - F$ with $x_0 \in]0, \rho[$. Then the correlation dimension of U_0 is zero.*

Proof. We assume that $\delta > 0$ is small and fixed. Since $x_n \to 0$, there exists $n_\delta \in \mathbb{N}$ such that $0 < x_n \le \delta$ for all $n > n_\delta$. This implies that

$$\frac{\binom{n-n_\delta}{2}}{\binom{n}{2}} \le C(n, \delta) \le 1, \quad \forall n > n_\delta + 1.$$

We conclude that $\ln C(n, \delta)$ tends to 0 as $n \to \infty$, for each fixed $\delta > 0$. This completes the proof. □

3 Balanced canard cycles in the orientable case

In this section we introduce two fractal methods (the one-sided dimension method and the fractal zeta-function method) for the detection of the number of limit cycles and the type of bifurcations Hausdorff close to balanced canard cycles with one breaking parameter. We focus on very general smooth planar slow-fast systems with a Hopf breaking mechanism or a jump breaking mechanism defined in [7]. We give a detailed study of the Hopf case. The study of the jump case is analogous to the study of the Hopf case (see [18]).

We deal with a smooth λ-family of slow-fast systems $X_{\epsilon,\lambda}$ where $\epsilon \geq 0$ is the singular parameter and $\lambda \sim \lambda_0 \in \mathbb{R}^m$ is a regular parameter. We assume that the dynamics of the fast subsystem $X_{0,\lambda}$ is given in Figure 2. More precisely, we have a critical curve with one normally attracting part, one normally repelling part and a Hopf turning point at T (sometimes called a generic turning point) between them. We say that $X_{\epsilon,\lambda}$ has a Hopf turning point at T at level $(\epsilon,\lambda) = (0,\lambda_0)$ if there exists a smooth coordinate change near T (preserving the parameter (ϵ,λ)) and a smooth regular change of time bringing $X_{\epsilon,\lambda}$ to

$$\left\{ \begin{array}{rcl} \dot{x} & = & y \\ \dot{y} & = & -xy + \epsilon\big(b(\lambda) - x + x^2\tilde{F}(x,\epsilon,\lambda)\big) + \epsilon y^2\tilde{G}(x,y,\epsilon,\lambda), \end{array} \right. \tag{5}$$

with smooth functions b, $\tilde{F}$ and $\tilde{G}$ near $(x,y) = (0,0)$ and $b(\lambda_0) = 0$. (If b is a submersion at $\lambda = \lambda_0$, then we can write $\lambda = (\tilde{b},\tilde{\lambda})$ and we call $\tilde{b} = b(\lambda) \sim 0$ the breaking parameter. We denote (5) by $X_{\epsilon,\tilde{b},\tilde{\lambda}}$ where $(\epsilon,\tilde{b},\tilde{\lambda}) \sim (0,0,\tilde{\lambda}_0)$.) Under the assumption about the contact point T, a passage from the attracting part to the repelling part near T is possible. To have a "global" passage from the

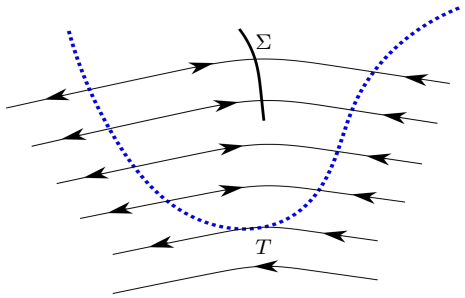

Figure 2: Canards with the Hopf breaking mechanism.

attracting part to the repelling part, we have to make an assumption about the slow dynamics of $X_{\epsilon,\lambda}$ along the critical curve, away from T. The slow dynamics is given by $x' = f(x,\lambda)$ where f is a smooth function, $\lambda \sim \lambda_0$ and the critical curve is parametrized by a regular parameter x. The attracting part (resp. the repelling part) is parametrized by $x > 0$ (resp. $x < 0$) and T is given by $x = 0$. We assume that $f < 0$ such that the dynamics near the critical curve points from the right to the left.

Now we can define the canard cycle Γ_s at level $(\epsilon,\lambda) = (0,\lambda_0)$ consisting of the fast orbit $s \in \Sigma$ and the part of the critical curve between the α-limit $x = \alpha(s,\lambda_0) < 0$ and the ω-limit $x = \omega(s,\lambda_0) > 0$ of the fast orbit. We may suppose without loss of generality that the transverse section Σ is parametrized by a regular parameter $s \sim 0$ (as s decreases, we are closer to T). All points of Σ lie in the basin of attraction (resp. repulsion) of the attracting part of the critical curve (resp. the repelling part). The slow relation function of $X_{\epsilon,\lambda}$ is an implicitly defined function G using

$$\int_{\alpha(s,\lambda)}^{\omega(G(s,\lambda),\lambda)} \frac{\operatorname{div} X_{0,\lambda} dx}{f(x,\lambda)} = 0, \quad (s,\lambda) \sim (0,\lambda_0). \tag{6}$$

If the canard cycle Γ_0 is balanced (i.e. $\int_{\alpha(0,\lambda_0)}^{\omega(0,\lambda_0)} \frac{\operatorname{div} X_{0,\lambda_0} dx}{f(x,\lambda_0)} = 0$), then the Implicit Function Theorem implies that the slow relation function G is well-defined and $G(0,\lambda_0) = 0$ because α and ω are smooth λ-families of diffeomorphisms and $\operatorname{div} X_{0,\lambda} < 0$ (resp. > 0) along the critical curve for $x > 0$ (resp. $x < 0$). From (6), it follows that $G'(0,\lambda_0) > 0$ (the derivative w.r.t. s). *In the rest of this section we suppose that* Γ_0 *is balanced.* For more details about the definition of the slow relation function and balanced canard cycles see e.g. [7].

The cyclicity of Γ_0, denoted by $\operatorname{Cycl}(\Gamma_0, X_{\epsilon,\lambda})$, is the maximum number of limit cycles of $X_{\epsilon,\lambda}$ in a fixed (Hausdorff) neighborhood of Γ_0, with $(\epsilon,\lambda) \sim (0,\lambda_0)$ and $\epsilon \geq 0$.

Theorem 3. *Suppose that* $F(s) := s - G(s,\lambda_0)$ *satisfies the conditions of Theorem 1 on* $[0,\rho[$ *where* G *is the slow relation function of* $X_{\epsilon,\lambda}$ *and* $\rho > 0$ *is small. Let* $U_0 = \{s_0, s_1, \dots\}$ *be the orbit of* $s_0 \in]0,\rho[$ *by* $G(s,\lambda_0)$ *and let* $U = \cup_{n=0}^{\infty}]s_{n+1}, s_n[$ *be a geometric realization of the fractal string* $\mathcal{S} = (s_n - s_{n+1})_{n=0}^{\infty}$. *Then the following statements are true:*

1. *If* $dim_B U_0 < 1$ *(resp.* $\Delta_{int}(U_0) < 1$, $D(\zeta_{\mathcal{S}}) < 1$*), then* $\operatorname{Cycl}(\Gamma_0, X_{\epsilon,\lambda}) \leq \frac{2-\dim_B U_0}{1-\dim_B U_0}$ *(resp.* $\operatorname{Cycl}(\Gamma_0, X_{\epsilon,\lambda}) \leq \frac{2-\Delta_{int}(U_0)}{1-\Delta_{int}(U_0)}$, $\operatorname{Cycl}(\Gamma_0, X_{\epsilon,\lambda}) \leq \frac{2-D(\zeta_{\mathcal{S}})}{1-D(\zeta_{\mathcal{S}})}$*).*

2. *If the function* $b(\lambda)$ *in (5) is a submersion at* $\lambda = \lambda_0$ *and* $\dim_B U_0 = \Delta_{int}(U_0) = D(\zeta_{\mathcal{S}}) = 0$, *then* $\operatorname{Cycl}(\Gamma_0, X_{\epsilon,\lambda}) = 2$ *and for each* $\epsilon > 0$ *and* $\tilde{\lambda} \sim \tilde{\lambda}_0$ *the* $\tilde{b}$*-family* $X_{\epsilon,\tilde{b},\tilde{\lambda}}$ *undergoes a saddle-node bifurcation of limit cycles Hausdorff close to* Γ_0.

3. *If the function* $b(\lambda)$ *in (5) is a submersion at* $\lambda = \lambda_0$ *and* $\dim_B U_0 = \Delta_{int}(U_0) = D(\zeta_{\mathcal{S}}) = 0$, *then there exists a continuous function* $\tilde{b}(\epsilon,\tilde{\lambda})$ *for* $\epsilon \geq 0$, *smooth for* $\epsilon > 0$ *and* $\tilde{b}(0,\tilde{\lambda}) = 0$ *such that* $X_{\epsilon,\tilde{b}(\epsilon,\tilde{\lambda}),\tilde{\lambda}}$ *has a unique limit cycle in Hausdorff sense close to* Γ_0 *for each* $\epsilon \sim 0$, $\epsilon > 0$ *and for each* $\tilde{\lambda} \sim \tilde{\lambda}_0$. *The limit cycle is hyperbolic and attracting.*

Following Theorem 3, we can choose one $s_0 > 0$ such that $s_0 \sim 0$ and generate the orbit U_0 of s_0 by $G(s,\lambda_0)$ by using the following recursive formula:

$$\int_{\alpha(s_n,\lambda_0)}^{\omega(s_{n+1},\lambda_0)} \frac{\operatorname{div} X_{0,\lambda_0} dx}{f(x,\lambda_0)} = 0,\ n = 0,1,2,\dots. \tag{7}$$

Then we compute the fractal dimensions of U_0 or the abscissa of convergence of the fractal-zeta function of U_0 and obtain the number of limit cycles near Γ_0. If the function F (i.e. G) does not satisfy the conditions of Theorem 1, we can replace $[\alpha(s_n,\lambda_0), \omega(s_{n+1},\lambda_0)]$ with $[\alpha(s_{n+1},\lambda_0), \omega(s_n,\lambda_0)]$ in (7) or, equivalently, we replace $X_{\epsilon,\lambda}$ with $-X_{\epsilon,\lambda}$ (for more details see [18]).

Theorem 3 will be proved in Section 6.1.1. Using Theorem 1 we can express the results of Theorem 3 in terms of the limit given in (2). We point out that the results in [18] can be expressed in terms of the one-sided dimension and the fractal zeta-function (we replace $dim_B U_0$ with $\Delta_{int}(U_0)$ and $D(\zeta_{\mathcal{S}})$). The same is true for the results in [20] where balanced canard cycles with two breaking parameters have been studied using the box dimension method.

4 Balanced canard cycles on a Möbius band

In this section we deal with a slow-fast model on a Möbius band introduced in [19]. For the sake of readability, we focus on canard cycles with a Hopf breaking mechanism (for generalizations see [19]). We denote a smooth Möbius band by N. Let $X_{\epsilon,\lambda}$ be a smooth (ϵ,λ)-family of vector fields on N where $\epsilon \geq 0$ is the singular perturbation parameter kept small and $\lambda \sim \lambda_0$ is a regular parameter. We suppose that $X_{\epsilon,\lambda}$ has a slow-fast Hopf point $T \in N$ for $(\epsilon,\lambda) = (0,\lambda_0)$, i.e. there exists a local chart on N around T in which $X_{\epsilon,\lambda}$ is given (up to a smooth equivalence) by (5) where b is a submersion at $\lambda = \lambda_0$. Sometimes we write $X_{\epsilon,\tilde{b},\tilde{\lambda}}$ instead of $X_{\epsilon,\lambda}$ where $(\epsilon,\tilde{b},\tilde{\lambda}) \sim (0,0,\tilde{\lambda}_0)$ and $\epsilon \geq 0$ (see Section 3). When

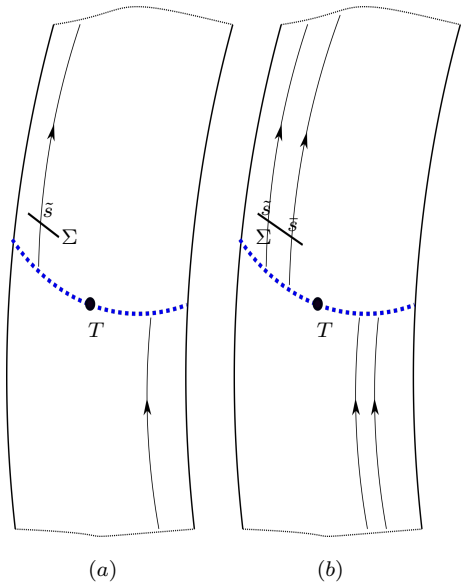

Figure 3: Two types of canard limit periodic sets on N at level $(\epsilon,\lambda) = (0,\lambda_0)$. (a) 1–canard cycles turning around N once. (b) 2–canard cycles turning around N twice.

$\epsilon = 0$, we assume that $X_{\epsilon,\lambda}$ has a smooth λ-family of one dimensional embedded critical manifolds (see Figure 3). We further assume that the slow dynamics $x' = f(x,\lambda)$ along the critical manifolds is nonzero pointing from the attracting part to the repelling part (like in Section 3, we use the regular parameter x). We distinguish between two types of limit periodic sets for $(\epsilon,\lambda) = (0,0)$ that can produce limit cycles in $X_{\epsilon,\lambda}$ after a perturbation: 1–canard cycles $\Gamma_{\tilde{s}}$ and 2–canard cycles $\Gamma_{\tilde{s},\bar{s}}$, $\tilde{s} < \bar{s}$, where the transverse section Σ is parametrized by a regular parameter s (without loss of generality we assume that s increases as we are closer to T). The canard cycle $\Gamma_{\tilde{s}}$ consists of the fast orbit of X_{0,λ_0} through $\tilde{s} \in \Sigma$ turning around the Möbius band N (once) and the part of the critical curve between the ω-limit $x = \omega(\tilde{s},\lambda_0) > 0$ and the α-limit $x = \alpha(\tilde{s},\lambda_0) < 0$ of the fast orbit. The canard cycle $\Gamma_{\tilde{s},\bar{s}}$ consists of the fast orbit of X_{0,λ_0} through $\tilde{s} \in \Sigma$ turning around N, the part of the critical curve between $x = \omega(\tilde{s},\lambda_0) > 0$ and $x = \alpha(\bar{s},\lambda_0) < 0$, the fast orbit of X_{0,λ_0} through $\bar{s} \in \Sigma$ turning around N and the part of the slow curve between $x = \omega(\bar{s},\lambda_0) > 0$ and $x = \alpha(\tilde{s},\lambda_0) < 0$.

We have $\omega(\tilde{s},\lambda_0) > \omega(\bar{s},\lambda_0)$ using a topological argument on N (see Definition 1 in [19]).

We denote by $\mathrm{Cycl}(\Gamma_{\tilde{s}}, X_{\epsilon,\lambda})$ (resp. $\mathrm{Cycl}(\Gamma_{\tilde{s},\bar{s}}, X_{\epsilon,\lambda})$) the cyclicity of $\Gamma_{\tilde{s}}$ (resp. $\Gamma_{\tilde{s},\bar{s}}$) in the family $X_{\epsilon,\lambda}$ with $(\epsilon,\lambda) \sim (0,\lambda_0)$ and $\epsilon \geq 0$. Following [16] or [19], $\mathrm{Cycl}(\Gamma_{\tilde{s}}, X_{\epsilon,\lambda})$ (resp. $\mathrm{Cycl}(\Gamma_{\tilde{s},\bar{s}}, X_{\epsilon,\lambda})$) is the maximum number of limit cycles turning around the Möbius band twice, Hausdorff close to $\Gamma_{\tilde{s}}$, $+1$ (resp. the maximum number of limit cycles turning around N twice, Hausdorff close to $\Gamma_{\tilde{s},\bar{s}}$).

Near $\Gamma_{\tilde{s}}$, we define a (unique) smooth slow relation function $G(s,\lambda)$ such that $G(\tilde{s},\lambda_0) = \tilde{s}$ and G satisfies (6) with $(s,\lambda) \sim (\tilde{s},\lambda_0)$. Here we have to assume that $\Gamma_{\tilde{s}}$ is balanced ($I(\tilde{s}) := \int_{\alpha(\tilde{s},\lambda_0)}^{\omega(\tilde{s},\lambda_0)} \frac{\mathrm{div}\, X_{0,\lambda_0} dx}{f(x,\lambda_0)} = 0$ where $\mathrm{div}\, X_{0,\lambda_0}$ is computed along the critical curve between $\alpha(\tilde{s},\lambda_0)$ and $\omega(\tilde{s},\lambda_0)$). We have

Theorem 4. *Suppose that $F(s) := s - G(s,\lambda_0)$ satisfies the conditions of Theorem 1 on $[\tilde{s},\tilde{s}+\rho[$ where G is the slow relation function near the balanced cycle $\Gamma_{\tilde{s}}$ and $\rho > 0$ is small. Let $U_0 = \{s_0, s_1, \dots\}$ be the orbit of $s_0 \in]\tilde{s},\tilde{s}+\rho[$ by $G(s,\lambda_0)$ and let $U = \cup_{n=0}^{\infty}]s_{n+1}, s_n[$ be a geometric realization of the fractal string $\mathcal{S} = (s_n - s_{n+1})_{n=0}^{\infty}$. If $\dim_B U_0 = \Delta_{int}(U_0) = D(\zeta_{\mathcal{S}}) = 0$, then the following statements are true:*

1. *There exist functions $s(\epsilon,\tilde{\lambda})$ and $\tilde{b}(\epsilon,\tilde{\lambda})$, continuous for $\epsilon \geq 0$ and $\tilde{\lambda} \sim \tilde{\lambda}_0$ and smooth for $\epsilon > 0$, with $s(0,\tilde{\lambda}_0) = \tilde{s}$ and $\tilde{b}(0,\tilde{\lambda}) = 0$ so that for each ϵ small and positive and $\tilde{\lambda} \sim \tilde{\lambda}_0$ the $\tilde{b}$-family $X_{\epsilon,\tilde{b},\tilde{\lambda}}$ undergoes a period doubling (or flip) bifurcation at $(s,\tilde{b}) = (s(\epsilon,\tilde{\lambda}), \tilde{b}(\epsilon,\tilde{\lambda}))$. The limit cycle turning around N twice and generated by the period doubling bifurcation is attracting.*

2. *We have $\mathrm{Cycl}(\Gamma_{\tilde{s}}, X_{\epsilon,\lambda}) = 2$ (there is one limit cycle turning around N once coexisting with at most one limit cycle turning around N twice, generated by the period doubling bifurcation).*

We prove Theorem 4 in Section 6.1.2. The recursive formula (7) can also be used here to generate the orbit U_0 near $\Gamma_{\tilde{s}}$.

We say that a 2–canard cycle $\Gamma_{\tilde{s},\bar{s}}$ is balanced if $I(\tilde{s}) = I(\bar{s}) = 0$. Then the slow relation functions G_1 near $\tilde{s}$ and G_2 near $\bar{s}$ are defined. We say that $\Gamma_{\tilde{s},\bar{s}}$ is semi-balanced if $I(\tilde{s}) \neq 0$ and $I(\bar{s}) = 0$. Then the slow relation function G_2 near $\bar{s}$ is well defined. We have

Theorem 5. *The following statements are true:*

1. *Let $\Gamma_{\tilde{s},\bar{s}}$ be balanced and let $F_1(s) := s - G_1(s,\lambda_0)$ (resp. $F_2(s) := s - G_2(s,\lambda_0)$) satisfy the conditions of Theorem 1 on $[\tilde{s},\tilde{s}+\rho[$ (resp. $[\bar{s},\bar{s}+\rho[$), where G_1 and G_2 are the slow relation functions of $\Gamma_{\tilde{s},\bar{s}}$ and $\rho > 0$ is small. Let $U_0^1 = \{s_0, s_1, \dots\}$ (resp. $U_0^2 = \{s_0, s_1, \dots\}$) be the orbit of $s_0 \in]\tilde{s},\tilde{s}+\rho[$ (resp. $s_0 \in]\bar{s},\bar{s}+\rho[$) by $G_1(s,\lambda_0)$ (resp. $G_2(s,\lambda_0)$) and let $U^1 = \cup_{n=0}^{\infty}]s_{n+1}, s_n[$ (resp. $U^2 = \cup_{n=0}^{\infty}]s_{n+1}, s_n[$) be a geometric realization of the fractal string $\mathcal{S}^1 = (s_n - s_{n+1})_{n=0}^{\infty}$ (resp. $\mathcal{S}^2 = (s_n - s_{n+1})_{n=0}^{\infty}$). If $\dim_B U_0^i = \Delta_{int}(U_0^i) = D(\zeta_{\mathcal{S}^i}) = 0$ for $i = 1, 2$, then $\mathrm{Cycl}(\Gamma_{\tilde{s},\bar{s}}, X_{\epsilon,\lambda}) \leq 2$.*

2. *Let $\Gamma_{\tilde{s},\bar{s}}$ be semi-balanced. Then $\mathrm{Cycl}(\Gamma_{\tilde{s},\bar{s}}, X_{\epsilon,\lambda}) \leq 1$ (the possible limit cycle is hyperbolic and attracting (resp. repelling) if $I(\tilde{s}) < 0$ (resp.*

$I(\tilde{s}) > 0$)). *Moreover, if* $\dim_B U_0^2 = \Delta_{int}(U_0^2) = D(\zeta_{\mathcal{S}^2}) = 0$, *then* $\mathrm{Cycl}(\Gamma_{\tilde{s},\bar{s}}, X_{\epsilon,\lambda}) = 1$ *where* U_0^2, U^2 *and* $\mathcal{S}^2$ *are defined in Theorem 5.1.*

3. *When* $\Gamma_{\tilde{s},\bar{s}}$ *is neither balanced nor semi-balanced, then* $\Gamma_{\tilde{s},\bar{s}}$ *produces no limit cycles.*

We prove Theorem 5 in Section 6.1.3.

5 The box dimension of slow-fast Hopf point

In the previous two sections we dealt with the slow-fast Hopf point (5) which turns out to be an important mechanism when we create canard cycles of size $O(1)$ and small amplitude limit cycles born from the slow-fast Hopf point. When dealing with the small limit cycles the cyclicity usually depends on the codimension of the slow-fast Hopf point (see e.g. [10]). *In this section we show that there exists a bijective correspondence between the codimension of the slow-fast Hopf point and the box dimension of one orbit of the (non-smooth) slow relation function, defined near the slow-fast Hopf point.* Here we rewrite (C^∞–) smooth system (5) in the form:

$$\begin{cases} \dot{x} &= y \\ \dot{y} &= -xy + \epsilon\big(b(\lambda) + \bar{F}(x,\epsilon,\lambda)\big) + \epsilon y^2 \tilde{G}(x,y,\epsilon,\lambda), \end{cases} \tag{8}$$

where $\bar{F}(x,\epsilon,\lambda) = -x + x^2\tilde{F}(x,\epsilon,\lambda)$. The Taylor expansion of $\bar{F}$ at $x = 0$ gives

$$j^\infty \bar{F}(x,\epsilon,\lambda) = -x + \sum_{i=2}^{\infty} f_i(\epsilon,\lambda)x^i$$

where j^∞ denotes the infinite jet. The system (8) has a finite codimension if there exists a nonzero even coefficient $f_{2k}(0,\lambda_0)$ (we call the smallest k with this property the codimension of the slow-fast Hopf point).

We take $\Sigma = \{x = 0\}$ parametrized by $y \geq 0$ and $y \sim 0$ where $y = 0$ corresponds to the slow-fast Hopf point $(x,y) = (0,0)$ where the normal hyperbolicity is lost (see Figure 2). Notice that the the origin is always balanced, i.e. $\int_{\alpha(0,\lambda_0)}^{\omega(0,\lambda_0)} \frac{\operatorname{div} X_{0,\lambda_0} dx}{f(x,\lambda_0)} = 0$, because $\alpha(0,\lambda_0) = \omega(0,\lambda_0) = 0$. (Using (8) it can be easily seen that $\alpha(y,\lambda) = -\sqrt{2y}$, $\omega(y,\lambda) = \sqrt{2y}$, $\operatorname{div} X_{0,\lambda} = -x$ and $f(x,\lambda) = \bar{F}(x,0,\lambda)/x$.) There exists a (unique) function $G(y,\lambda)$ such that (6) holds for each $s = y \geq 0$, $y \sim 0$ and $\lambda \sim \lambda_0$. This follows from the fact that the integrand in (6) changes sign as x passes through the origin. The degree of smoothness of G at $y = 0$ increases as the codimension of the slow-fast Hopf point increases (see Theorem 6). We assume that the (balanced) origin is isolated, i.e. $\int_{\alpha(y,\lambda_0)}^{\omega(y,\lambda_0)} \frac{\operatorname{div} X_{0,\lambda_0} dx}{f(x,\lambda_0)} \neq 0$ for all $y > 0$ and $y \sim 0$ (thus, Γ_y is not balanced for all positive $y \sim 0$). For example, this is the case when the codimension is finite (see Theorem 6). Without loss of generality we take the above integral to be positive for all small $y > 0$: then any orbit generated by G is decreasing and tends to $y = 0$ (in the finite codimension case this corresponds to $f_{2k}(0,\lambda_0) > 0$, see the proof of Theorem 6). If (8) is analytic of infinite codimension, then the origin is not isolated (i.e. $G(y,\lambda_0) = y$ for all $y \geq 0$) because the integrand function $\frac{\operatorname{div} X_{0,\lambda_0}}{f(x,\lambda_0)}$ is odd.

Theorem 6. *Let G be the slow relation function with $y \geq 0$ and $y \sim 0$ as defined above and let $U_0 = \{y_0, y_1, \dots\}$ be the orbit of a small $y_0 > 0$ by $G(y, \lambda_0)$ tending monotonically to zero. If the codimension of the slow-fast Hopf point (8) is finite and equal to k, then $G(y, \lambda_0)$ is of class C^k in y, including $y = 0$, $y - G(y, \lambda_0) \simeq y^{\frac{2k+1}{2}}$, as $y \to 0$, and $dim_B U_0 = \frac{2k-1}{2k+1}$. When the system (8) is of infinite codimension, then $G(y, \lambda_0)$ is of class C^∞, including $y = 0$, and $dim_B U_0 = 1$.*

We prove Theorem 6 in Section 6.2. Following Theorem 6, the box dimension of the slow relation function $G(y, \lambda_0)$ attached to the slow-fast Hopf point can take only the following discrete set of values: $\frac{1}{3}, \frac{3}{5}, \frac{5}{7}, \dots, 1$.

When $\tilde{G} \equiv 0$, small limit cycles of the Liénard system (8) have been studied in [10]. The main result in [10] is that there is a finite upper bound for the number of small limit cycles if (8) is smooth with a finite codimension or analytic. If the codimension is k, then the cyclicity is bounded by k, up to a conjecture on Abelian integrals. The conjecture has been solved for $k \leq 2$ (see [13]). In [10], the authors work with (8) in the Liénard plane $\{\dot{x} = y - O(x^2), \dot{y} = \epsilon(b - x)\}$ (there exists a smooth (resp. analytic) equivalence) and the codimension is then related to the first nonzero odd coefficient in the $O(x^2)$-term. For more details, see [10].

The system (8) with codimension 1 has been studied in [9, 21].

6 Proof of Theorems 3–6

6.1 Canard cycles

Let $X_{\epsilon,\lambda}$ be the family defined in Section 3 or Section 4. We define the slow divergence integral along the attracting part of the critical curve

$$I_-(s, \lambda) := \int_{\omega(s,\lambda)}^{0} \frac{\operatorname{div} X_{0,\lambda} dx}{f(x, \lambda)} < 0, \quad (s, \lambda) \sim (s^0, \lambda_0),$$

and along the repelling part of the critical curve

$$I_+(s, \lambda) := \int_{\alpha(s,\lambda)}^{0} \frac{\operatorname{div} X_{0,\lambda} dx}{f(x, \lambda)} < 0, \quad (s, \lambda) \sim (s^0, \lambda_0),$$

where $s^0 = 0$ (resp. $s^0 = \tilde{s}$ or $s^0 = \bar{s}$) if we deal with the slow-fast model in Section 3 (resp. Section 4). A smooth function $\kappa_1(s, \lambda)$ is C^∞-contact equivalent to a smooth function $\kappa_2(s, \lambda)$ if there exists a nowhere zero smooth function $\Omega(s, \lambda)$ such that $\kappa_1(s, \lambda) = \Omega(s, \lambda)\kappa_2(s, \lambda)$ (let's recall that smooth means C^∞-smooth). It can be easily seen that in the case of C^∞-contact equivalence $s = s^0$ is a zero of multiplicity l of $\kappa_1(s, \lambda_0)$ if and only if $s = s^0$ is a zero of multiplicity

l of $\kappa_2(s,\lambda_0)$. We have for $(s,\lambda)\sim(s^0,\lambda_0)$

$$\begin{aligned} I_-(s,\lambda)-I_+(s,\lambda) &= -\int_{\alpha(s,\lambda)}^{\omega(s,\lambda)} \frac{\operatorname{div} X_{0,\lambda}dx}{f(x,\lambda)} \\ &= \int_{\alpha(s,\lambda)}^{\omega(G(s,\lambda),\lambda)} \frac{\operatorname{div} X_{0,\lambda}dx}{f(x,\lambda)} - \int_{\alpha(s,\lambda)}^{\omega(s,\lambda)} \frac{\operatorname{div} X_{0,\lambda}dx}{f(x,\lambda)} \\ &= \int_{\omega(s,\lambda)}^{\omega(G(s,\lambda),\lambda)} \frac{\operatorname{div} X_{0,\lambda}dx}{f(x,\lambda)} \end{aligned}$$

where G is the slow relation function. In the second line we used (6). From here it follows that $I_-(s,\lambda)-I_+(s,\lambda)$ is C^∞-contact equivalent to $s-G(s,\lambda)$ because the integrand in the last integral is positive and ω is a λ-family of smooth diffeomorphisms w.r.t. s.

6.1.1 Proof of Theorem 3

Suppose that the assumption about G of Theorem 3 is satisfied. If $dim_B U_0 < 1$ (resp. $\Delta_{int}(U_0) < 1$, $D(\zeta_{\mathcal{S}}) < 1$), then $l = \frac{1}{1-dim_B U_0}$ (resp. $l = \frac{1}{1-\Delta_{int}(U_0)}$, $l = \frac{1}{1-D(\zeta_{\mathcal{S}})}$) where l is the multiplicity of the zero $s=0$ of $F(s) := s - G(s,\lambda_0)$. (See Theorem 1.1 and Theorem 2.2.) Then the multiplicity of $s=0$ of $I_-(s,\lambda_0)-I_+(s,\lambda_0)$ is also l and we have that $\mathrm{Cycl}(\Gamma_0, X_{\epsilon,\lambda}) \le l+1$ (see e.g. [7]). This completes the proof of Theorem 3.1. Theorem 3.2 and Theorem 3.3 have been proved in [18] for $dim_B U_0$. It suffices to notice that $\dim_B U_0 = \Delta_{int}(U_0) = D(\zeta_{\mathcal{S}})$ (see Theorem 2.1).

6.1.2 Proof of Theorem 4

Suppose that the assumption about G of Theorem 4 is satisfied. Since $\dim_B U_0 = \Delta_{int}(U_0) = D(\zeta_{\mathcal{S}}) = 0$, we have that $s=\tilde{s}$ is a zero of multiplicity 1 of $s - G(s,\lambda_0)$ (and thus of $I_-(s,\lambda_0)-I_+(s,\lambda_0)$). Now, Theorem 4.1 (resp. Theorem 4.2) follows from Theorem 2.3 (resp. Theorem 2.4) in [19].

6.1.3 Proof of Theorem 5

Like in Section 6.1.2, it can be easily seen that Theorem 5 follows from Theorem 2.7 in [19].

6.2 The slow-fast Hopf point and proof of Theorem 6

Suppose that the codimension of the system (8) is finite and equal to k. Using the notation from Section 6.1 we have for small $y \ge 0$:

$$I_-(y,\lambda_0)-I_+(y,\lambda_0) = \int_{-\sqrt{2y}}^{\sqrt{2y}} \frac{xdx}{-1+\sum_{i=1}^{k-1} f_{2i+1}x^{2i} + f_{2k}x^{2k-1} + O(x^{2k})}.$$

where we write $f_i = f_i(0,\lambda_0)$. In the above integral, the integrand function can be written as:

$$\frac{x}{-1+\sum_{i=1}^{k-1} f_{2i+1}x^{2i}} - f_{2k}x^{2k} + O(x^{2k+1}). \tag{9}$$

Since the first term in (9) is an odd function, we have

$$I_-(y,\lambda_0) - I_+(y,\lambda_0) = -f_{2k}\frac{2^{\frac{2k+3}{2}}}{2k+1}(\sqrt{y})^{2k+1} + O\big((\sqrt{y})^{2k+2}\big). \tag{10}$$

On the other hand, using Section 6.1 and writing $G(y) = G(y,\lambda_0)$ we get

$$\begin{aligned} I_-(y,\lambda_0) - I_+(y,\lambda_0) &= -\int_{\sqrt{2y}}^{\sqrt{2G(y)}} \frac{x\,dx}{-1+\sum_{i=1}^{k-1} f_{2i+1}x^{2i} + f_{2k}x^{2k-1} + O(x^{2k})} \\ &= -\int_{y}^{G(y)} \frac{ds}{-1+\sum_{i=1}^{k-1} f_{2i+1}(2s)^{i} + f_{2k}(2s)^{\frac{2k-1}{2}} + O((2s)^{k})} \end{aligned} \tag{11}$$

where the $O((2s)^k)$-term is smooth in $\sqrt{s}$. In the last step we used the coordinate change $x^2 = 2s$. Since the integrand function in (11) is continuous (more precisely, C^{k-1}) and uniformly negative, the Mean Value Theorem for Integrals and (10) imply that $y - G(y) \simeq y^{\frac{2k+1}{2}}$, as $y \to 0$, if $f_{2k} > 0$. (If $f_{2k} < 0$, then the orbit generated by $G(y)$ is repelling). From $\alpha := \frac{2k+1}{2} > 1$ and Theorem 1 in [11] follows that $\dim_B U_0 = 1 - \frac{1}{\alpha}$. The C^k-smoothness of $G(y)$ in $y = 0$ follows from (10), (11) and the C^k-version of the Implicit Function Theorem.

When (8) is of infinite codimension then for any $k = 1, 2, \dots$ we have that $I_-(y,\lambda_0) - I_+(y,\lambda_0) = O\big((\sqrt{y})^{2k+2}\big)$ (see (10)) and that (11) holds with $f_{2k} = 0$. Thus, for any k we have that $y - G(y) = O\big((\sqrt{y})^{2k+2}\big)$. Following Theorem 6 of [11], we conclude that $\dim_B U_0 = 1$. Using the Implicit Function Theorem for each k, we get the C^∞-smoothness of G in $y \geq 0$.

7 The speed of convergence and applications

7.1 Comparing the speed of convergence of the fractal methods

In this section we suppose that $F : [0, \rho[\to \mathbb{R}$ satisfies the assumptions given in Theorem 1 and that $l \in \{2, 3, \dots\}$ (for the case where $l = 1$ or $l = \infty$ see Remark 5). Then $F(x) \simeq x^l$ as $x \to 0$ with positive constants C and D (see Section 2.1). Let U_0 be the orbit of x_0 by $id - F$ with x_0 small and positive. Following Theorem 1 from [11], we know that $x_n \simeq n^{-\frac{1}{l-1}}$ as $n \to \infty$ with two positive constants c and d. Our goal is to estimate $\dim_B U_0$ by using the limits in (2), (3) and (4) and a finite number of elements in U_0. We denote the sequence in (2), (3) or (4) by $(a_n)_{n=0}^\infty$. For a given κ small and positive we want to find $n_0 \in \mathbb{N}$ such that $a_n \in [\dim_B U_0 - \kappa, \dim_B U_0 + \kappa]$ for all $n \geq n_0$.

Lemma 1. *Let F and U_0 be as defined above and $\kappa > 0$ small. Then the following statements are true.*

1. *If $(a_n)_{n=0}^\infty$ denotes the sequence in (2), then we have*

$$n_0 = \lceil \max\left\{ (Cc^l)^{\frac{l-1}{l} - \frac{(l-1)^2}{l^2\kappa}}, (Dd^l)^{\frac{l-1}{l} + \frac{(l-1)^2}{l^2\kappa}} \right\} \rceil. \tag{12}$$

2. *If $(a_n)_{n=0}^\infty$ denotes the sequence in (3), then we have*

$$n_0 = \lceil \max\left\{ c^{\frac{l-1}{l} - \frac{(l-1)^2}{l^2\kappa}}, d^{\frac{l-1}{l} + \frac{(l-1)^2}{l^2\kappa}} \right\} \rceil. \tag{13}$$

3. If $(a_n)_{n=0}^{\infty}$ denotes the sequence in (4), then we have

$$n_0 = \lceil \max \left\{ \frac{(\frac{Dd^l}{2})^{(\frac{1}{l}+\kappa)\frac{l-1}{l\kappa}}}{(Cc^l+c)^{\frac{l-1}{l\kappa}}}, \frac{(Dd^l+d)^{\frac{l-1}{l\kappa}}}{(\frac{Cc^l}{2})^{(\frac{1}{l}-\kappa)\frac{l-1}{l\kappa}}} \right\} \rceil. \tag{14}$$

Proof. We use $Cx^l \leq F(x) \leq Dx^l$, $cn^{-\frac{1}{l-1}} \leq x_n \leq dn^{-\frac{1}{l-1}}$, $x_n - x_{n+1} = F(x_n)$ and $\dim_B U_0 = \frac{l-1}{l}$.
Statement 1. We write $a_n = \frac{\ln n}{-\ln F(x_n)}$. Then $a_n \geq \dim_B U_0 - \kappa$ is true if $\ln n \geq -(\frac{l-1}{l} - \kappa)\ln(Cc^l n^{-\frac{l}{l-1}})$, or equivalently, $n \geq (Cc^l)^{\frac{l-1}{l} - \frac{(l-1)^2}{l^2\kappa}}$. Similarly, $a_n \leq \dim_B U_0 + \kappa$ if $\ln n \leq -(\frac{l-1}{l} + \kappa)\ln(Dd^l n^{-\frac{l}{l-1}})$, or equivalently, $n \geq (Dd^l)^{\frac{l-1}{l} + \frac{(l-1)^2}{l^2\kappa}}$.
Statement 2. We have $a_n = \frac{1}{1 - \frac{\ln x_n}{\ln n}}$. Then $a_n \geq \dim_B U_0 - \kappa$ is equivalent to $x_n^{\frac{l-1}{l}-\kappa} \geq n^{-(\frac{1}{l}+\kappa)}$. This is true if $c^{\frac{l-1}{l}-\kappa} n^{-\frac{1}{l}+\frac{\kappa}{l-1}} \geq n^{-(\frac{1}{l}+\kappa)}$, or equivalently, $n \geq c^{\frac{l-1}{l} - \frac{(l-1)^2}{l^2\kappa}}$. The study of $a_n \leq \dim_B U_0 + \kappa$ is similar to the study of $a_n \geq \dim_B U_0 - \kappa$.
Statement 3. We have $a_n = 1 - \frac{\ln(nF(x_n)+x_n)}{\ln \frac{F(x_n)}{2}}$. Then $a_n \geq \dim_B U_0 - \kappa$ is equivalent to $(\frac{F(x_n)}{2})^{\frac{1}{l}+\kappa} \leq nF(x_n)+x_n$. This is true if $(\frac{Dd^l n^{-\frac{l}{l-1}}}{2})^{\frac{1}{l}+\kappa} \leq (Cc^l + c)n^{-\frac{1}{l-1}}$, or equivalently, $n \geq \frac{(\frac{Dd^l}{2})^{(\frac{1}{l}+\kappa)\frac{l-1}{l\kappa}}}{(Cc^l+c)^{\frac{l-1}{l\kappa}}}$. The study of $a_n \leq \dim_B U_0 + \kappa$ is similar to the study of $a_n \geq \dim_B U_0 - \kappa$. □

We denote by $\mathcal{M}_1$ (resp. $\mathcal{M}_2$ and $\mathcal{M}_3$) the method for the estimation of $\dim_B U_0$ using the limit in (2) (resp. (3) and (4)). In order to compare the speed of convergence of $\mathcal{M}_1$, $\mathcal{M}_2$ and $\mathcal{M}_3$, we make some natural assumptions on the constants c, d, C and D. From the proof of Theorem 1 in [11] we know the bounds on c and d: $c \leq (\frac{1}{D(l-1)})^{\frac{1}{l-1}}$ and $d \geq (\frac{1}{C(l-1)})^{\frac{1}{l-1}}$. Since we can choose the constants C and D to be arbitrarily close, up to shrinking ρ, we assume that $C = D$. Moreover, we assume that c and d equal the above bounds, i.e. $c = d = (\frac{1}{C(l-1)})^{\frac{1}{l-1}}$ (see Remark 2 from [11]). This enables us to simplify the expressions in Lemma 1.

Lemma 2. *Suppose that $C = D$ and $c = d = (\frac{1}{C(l-1)})^{\frac{1}{l-1}}$ in Lemma 1. Then the following statements are true.*

1. In method $\mathcal{M}_1$ we have

$$n_0^{\mathcal{M}_1} = \lceil \max \left\{ \left(C^{\frac{1}{l}}(l-1) + O(\kappa) \right)^{\frac{l-1}{l\kappa}}, \left(\frac{1}{C^{\frac{1}{l}}(l-1)} + O(\kappa) \right)^{\frac{l-1}{l\kappa}} \right\} \rceil.$$

2. In method $\mathcal{M}_2$ we have

$$n_0^{\mathcal{M}_2} = \lceil \max \left\{ \left(C^{\frac{1}{l}}(l-1)^{\frac{1}{l}} + O(\kappa) \right)^{\frac{l-1}{l\kappa}}, \left(\frac{1}{C^{\frac{1}{l}}(l-1)^{\frac{1}{l}}} + O(\kappa) \right)^{\frac{l-1}{l\kappa}} \right\} \rceil.$$

3. In method $\mathcal{M}_3$ we have

$$n_0^{\mathcal{M}_3} = \lceil \max \left\{ \left(\frac{C^{\frac{1}{l}}(l-1)}{2^{\frac{1}{l}}l} + O(\kappa) \right)^{\frac{l-1}{l\kappa}}, \left(\frac{2^{\frac{1}{l}}l}{C^{\frac{1}{l}}(l-1)} + O(\kappa) \right)^{\frac{l-1}{l\kappa}} \right\} \rceil.$$

Proof. This follows directly from Lemma 1. □

The functions $n_0^{\mathcal{M}_1}$, $n_0^{\mathcal{M}_2}$ and $n_0^{\mathcal{M}_3}$ from Lemma 2 are well defined for all (l, C, κ) with $l > 1$, $C > 0$ and $\kappa \sim 0$ and $\kappa > 0$. Our goal is to compare the bases of the exponential terms in $n_0^{\mathcal{M}_1}$, $n_0^{\mathcal{M}_2}$ and $n_0^{\mathcal{M}_3}$ and to find which method has the fastest convergence, depending on (l, C)-values. In order to state the result, we define the following curves in the (l, C)-space: $\mathcal{C}_{12}^1 = \{C = \frac{1}{(l-1)^{\frac{l+1}{2}}}\}$, $\mathcal{C}_{12}^2 = \{l = 2\}$, $\mathcal{C}_{13} = \{C = \frac{\sqrt{2l^l}}{(l-1)^l}\}$ and $\mathcal{C}_{23} = \{C = \frac{\sqrt{2l^l}}{(l-1)^{\frac{l+1}{2}}}\}$ (see Figure 4). The curve $\mathcal{C}_{12}^1$ (resp. $\mathcal{C}_{12}^2$) is defined by equalizing the base of the first exponential term in $n_0^{\mathcal{M}_1}$ to the base of the second (resp. first) exponential term in $n_0^{\mathcal{M}_2}$, for $\kappa = 0$. Similarly, the curve $\mathcal{C}_{13}$ (resp. $\mathcal{C}_{23}$) is defined by equalizing the base of the first exponential term in $n_0^{\mathcal{M}_1}$ (resp. $n_0^{\mathcal{M}_2}$) to the base of the second exponential term in $n_0^{\mathcal{M}_3}$, for $\kappa = 0$. (When we equalize the base of the first exponential term in $n_0^{\mathcal{M}_1}$ (resp. $n_0^{\mathcal{M}_2}$) to the base of the first exponential term in $n_0^{\mathcal{M}_3}$, we get the empty set.) These curves divide the set

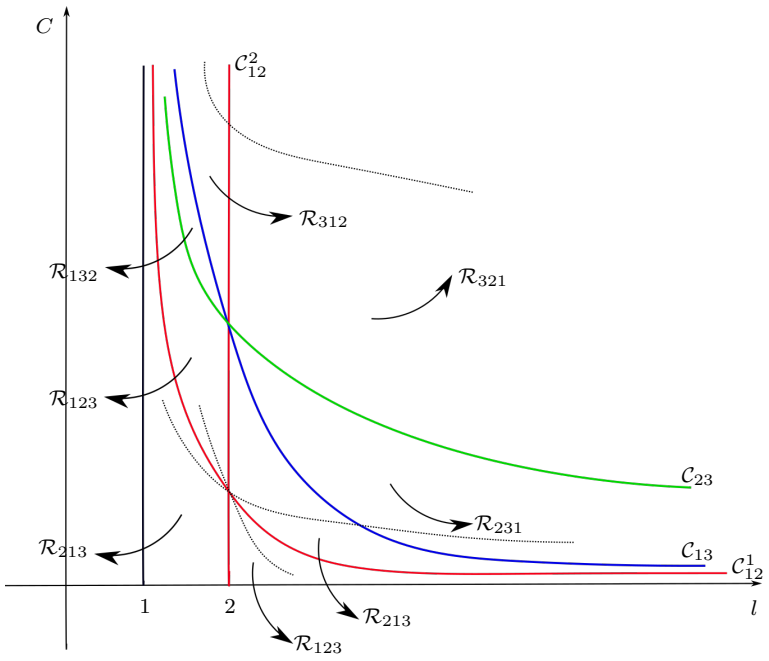

Figure 4: Three methods for the computation of $\dim_B U_0$: $\mathcal{M}_1$, $\mathcal{M}_2$ and $\mathcal{M}_3$. Comparing the bases of the exponential expressions in $n_0^{\mathcal{M}_1}$, $n_0^{\mathcal{M}_2}$ and $n_0^{\mathcal{M}_3}$ we see that in $\mathcal{R}_{ijk}$ the method $\mathcal{M}_i$ converges faster than $\mathcal{M}_j$ and that $\mathcal{M}_j$ converges faster than $\mathcal{M}_k$.

$\{l > 1, C > 0\}$ into 8 open regions. We denote them by $\mathcal{R}_{ijk}$ where ijk is a permutation of 123. Notice that $\mathcal{R}_{123}$ and $\mathcal{R}_{213}$ occur twice in Figure 4. In $\mathcal{R}_{ijk}$ we have $n_0^{\mathcal{M}_i} < n_0^{\mathcal{M}_j} < n_0^{\mathcal{M}_k}$, i.e. $\mathcal{M}_i$ converges faster than $\mathcal{M}_j$ and $\mathcal{M}_j$ converges faster than $\mathcal{M}_k$. More precisely,

Proposition 2. *Suppose that the assumptions of Lemma 2 are satisfied. For any compact set $\mathcal{K}$ in $\mathcal{R}_{ijk}$ there exists $\kappa_0 > 0$ such that $n_0^{\mathcal{M}_i} < n_0^{\mathcal{M}_j} < n_0^{\mathcal{M}_k}$ for all $(l, C) \in \mathcal{K}$ and $\kappa \in]0, \kappa_0]$.*

Proof. We prove the proposition for $\mathcal{R}_{123}$ bounded by $\mathcal{C}_{12}^1$, $\mathcal{C}_{12}^2$ and $C = 0$, i.e. $\mathcal{R}_{123} = \{l > 2, 0 < C < \frac{1}{(l-1)^{\frac{l+1}{2}}}\}$. The other cases can be treated in a similar way. We have $C^{\frac{1}{l}}(l-1) < \frac{1}{C^{\frac{1}{l}}(l-1)^{\frac{1}{l}}}$ and, because $l > 2$, $\frac{1}{C^{\frac{1}{l}}(l-1)} < \frac{1}{C^{\frac{1}{l}}(l-1)^{\frac{1}{l}}}$ and therefore $n_0^{\mathcal{M}_1} < n_0^{\mathcal{M}_2}$. On the other hand, we have $C^{\frac{1}{l}}(l-1)^{\frac{1}{l}} < \frac{2^{\frac{1}{l}} l}{C^{\frac{1}{l}}(l-1)}$ ($\mathcal{R}_{123}$ is located under $\mathcal{C}_{23}$) and $\frac{1}{C^{\frac{1}{l}}(l-1)^{\frac{1}{l}}} < \frac{2^{\frac{1}{l}} l}{C^{\frac{1}{l}}(l-1)}$ (because $(l-1)^{l-1} < 2l^l$). Thus, $n_0^{\mathcal{M}_2} < n_0^{\mathcal{M}_3}$. □

Remark 4. *Looking at the exponent of the exponential terms in Lemma 2 it is not difficult to see that the error κ decreases at a rate of $O(\frac{1}{\ln n})$ if the base is different from 1. When the base in $n_0^{\mathcal{M}_i}$ ($i = 1, 2, 3$) is equal to 1 at level $\kappa = 0$, we get a curve in the (l, C)-space along which $a_n - \dim_B U_0$ is flat if we expand it w.r.t. $\frac{1}{\ln n}$ (see three dotted curves in Figure 4).*

Remark 5. *Suppose that $l = 1$ and that the functions F and G satisfy the conditions of Theorem 1. We compare the methods $\mathcal{M}_1$, $\mathcal{M}_2$ and $\mathcal{M}_3$. For the sake of simplicity and readability, we will restrict ourselves to $G(x) = \alpha x$ where $\alpha \in]0, 1[$ (resp. $G(x) = Mx^\beta$ with $\beta \in \mathbb{N}$, $\beta > 1$ and $M > 0$) when $F'(0) < 1$ (resp. $F'(0) = 1$). In both cases we show that there exists $n_0 \in \mathbb{N}$ such that $0 < a_n^{\mathcal{M}_2} < a_n^{\mathcal{M}_1} < a_n^{\mathcal{M}_3}$ for all $n \geq n_0$ where $a_n^{\mathcal{M}_1}$ (resp. $a_n^{\mathcal{M}_2}$ and $a_n^{\mathcal{M}_3}$) is the sequence in (2) (resp. (3) and (4)). (Let us recall that these sequences tend to zero as $n \to \infty$ because $l = 1$.) Indeed, it is not difficult to see that $x_n = \alpha^n x_0$ (resp. $x_n = M^{\frac{\beta^n - 1}{\beta - 1}} x_0^{\beta^n}$). If we substitute this expression for x_n in (2) and (3), we have that $a_n^{\mathcal{M}_2} < a_n^{\mathcal{M}_1}$ for $n > \frac{1}{1-\alpha}$ (resp. for all n with $n\big(1 - (Mx_0^{\beta-1})^{\beta^n}\big) > 1$). We may assume that $Mx_0^{\beta-1} < 1$ by taking $x_0 > 0$ small and fixed. If we substitute x_n in (2) and (4), we have that $a_n^{\mathcal{M}_1} < a_n^{\mathcal{M}_3}$ is equivalent to*

$$\frac{\ln\big((1-\alpha)\alpha^n x_0\big) \ln \frac{n}{2n + \frac{2}{1-\alpha}}}{\ln 2 \ln n} > 1$$

$$\left(\text{resp. } \frac{\ln\big(M^{\frac{\beta^n - 1}{\beta - 1}} x_0^{\beta^n}(1 - (Mx_0^{\beta-1})^{\beta^n})\big) \ln \frac{n}{2n + \frac{2}{1 - (Mx_0^{\beta-1})^{\beta^n}}}}{\ln 2 \ln n} > 1\right).$$

Now, it suffices to notice that the expressions $-\frac{\ln \alpha^n}{\ln n}$ and $-\frac{\ln (M^{\frac{1}{\beta-1}} x_0)^{\beta^n}}{\ln n}$ tend to ∞ as $n \to \infty$. Thus, the method $\mathcal{M}_2$ produces the smallest error and the method $\mathcal{M}_3$ the biggest error. We expect it from Figure 4 when $l \to 1$. It can be easily seen that κ decreases at a rate of $O(\frac{\ln n}{n})$ (resp. $O(\frac{\ln n}{\beta^n})$) in (2), (3) and (4).

Figure 4 suggests that $\mathcal{M}_3$ can be used to compute the box dimension when $l \to \infty$. It is more difficult to compare the methods $\mathcal{M}_1$, $\mathcal{M}_2$ and $\mathcal{M}_3$ in the limit $l = \infty$. In the slow-fast setting we will always deal with systems where $l < \infty$ such that Theorem 3 can be applied (see Section 7.3).

7.2 Numerical validation of methods

In Lemma 2, Proposition 2 and for comparison of methods in Figure 4 we make (natural) assumptions on C, D, c and d. This is necessary if we want to make simple decision on the choice of the best method regarding only two parameters C and l. On the other hand, there does not exist a single function F satisfying these ideal conditions, as these conditions correspond to a limiting case (see Remark 2 from [11]). For this reason we choose to supplement our theoretical results with numerical experiments that validate the relevance of Lemma 2 and Proposition 2 in choosing the optimal method $\mathcal{M}_1$, $\mathcal{M}_2$ and $\mathcal{M}_3$ for a given problem.

7.2.1 Numerical reconstruction of regions $\mathcal{R}_{ijk}$

We reconstruct the regions $\mathcal{R}_{ijk}$ from Figure 4 by using only numerical estimation of the box dimension of sequence $U_0 = (x_n)_{n=0}^{\infty}$, where $x_{n+1} = x_n - F(x_n)$ for $F(x) = Cx^l$. More precisely, for the method $\mathcal{M}_1$ (resp. $\mathcal{M}_2$ and $\mathcal{M}_3$) we estimate $\dim_B U_0$, that is, the limit in (2) (resp. (3) and (4)) by computing limit expressions for some fixed large $n = n_0$. Also, we fix small $x_0 > 0$ and compute the orbit U_0 up to x_{n_0}-term. This way $\dim_B U_0 = \dim_B U_0(l, C)$ is estimated for every method and every pair of parameters (l, C) taken from a regular uniform compact grid.

On the other hand, from Theorem 1 in [11] we know the exact value of $\dim_B U_0(l, C)$ to be equal to $(l-1)/l$. Let $\kappa_{\mathcal{M}_1}(l, C)$ (resp. $\kappa_{\mathcal{M}_2}(l, C)$ and $\kappa_{\mathcal{M}_3}(l, C)$) be the Euclidean distance between the theoretical dimension $(l-1)/l$ and numerically estimated dimension for the method $\mathcal{M}_1$ (resp. $\mathcal{M}_2$ and $\mathcal{M}_3$). We say that the point (l, C) is in numerically reconstructed region $\mathcal{R}'_{ijk}$ if $\kappa_{\mathcal{M}_i}(l, C) < \kappa_{\mathcal{M}_j}(l, C) < \kappa_{\mathcal{M}_k}(l, C)$.

Finally, if the conditions of Lemma 2 and Proposition 2 are natural for choosing the optimal method, given parameters l and C, then the numerically reconstructed regions $\mathcal{R}'_{ijk}$ should qualitatively coincide with the theoretical regions $\mathcal{R}_{ijk}$ computed from Lemma 2. Figure 5 indicates that for numerical applications where we expect $l \geq 5$, method $\mathcal{M}_3$ is optimal for almost every value of C. For small l, method $\mathcal{M}_2$ is optimal for every valid C.

For the comparison of error estimates κ computed from Lemma 2 for a fixed n_0 and truly obtained numerical errors between theoretical end numerically estimated box dimensions for a selected values of l and C, see Table 1. It clearly illustrates that for smaller values of l, error estimates from Lemma 2 are very close to true obtained errors. For bigger values of l this error estimates are less useful. Fortunately, important application of our numerical method is in situations where l is small, see Section 7.3.

7.2.2 Implementation details

All numerical computations are developed in Wolfram Mathematica 11.1. Our code is available online at `https://github.com/FRABDYN/FractalDimensions`. All calculations are regarded as essentially interval calculations using Mathematica built-in automatic numerical precision control. Depending on concrete values of l and C, required precision was significantly greater than standard floating point double precision. In the worst case, in order to calculate data for Figure 5, we used maximum precision of 150 decimal places. The reason

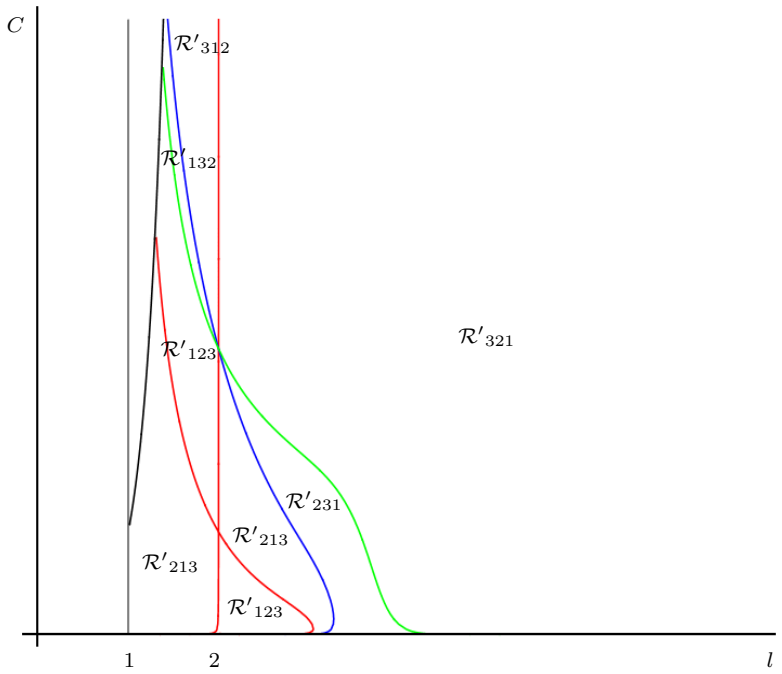

Figure 5: Numerically reconstructed regions $\mathcal{R}'_{ijk}$. Points (l, C) are sampled from intervals $l \in]1, 8]$ and $C \in]0, 6]$, with a maximum resolution of 0.05. For this figure n_0 is fixed at 10^5 and x_0 is fixed at 10^{-2}. Regions $\mathcal{R}'_{ijk}$ exist only where $x_0 \geq F(x_0)$, which means for $C \leq x_0^{-(l-1)}$.

is behind subtractions of close numerical values in formulas (2) and (4), where the number of significant digits is greatly reduced. This effect is much more pronounced for larger values of l and smaller values of x_0, when the speed of convergence of orbit U_0 becomes slower.

7.3 Application to classical Liénard equations of degree 6

In this section we use our box dimension approach and the numerical fractal methods from Section 7.1 to show the existence of a classical Liénard equation of degree 6 *with* 4 *(canard) limit cycles.* As explained in Section 1, this is a counterexample to the conjecture of Lins, de Melo and Pugh. We use the family of Liénard equations of degree 6 introduced in [4]:

$$\begin{cases} \dot{x} &= y - \left(\frac{1}{2}x^2 + 5\delta x^3 - \frac{35}{46}x^4 - 12\delta x^5 + \frac{21}{46}x^6\right) \\ \dot{y} &= \epsilon(b - x) \end{cases} \tag{15}$$

where $\epsilon \geq 0$ is the singular perturbation parameter kept small and $(b, \delta) \sim (0, 0)$. By studying the zeros of the slow divergence integral of (15) it has been proved that (see Theorem 1 in [4]):

Theorem 7. *Given $k \in \{1, 2, 3, 4\}$, there exists a smooth curve $b = \epsilon\mathcal{B}_k(\epsilon, \delta)$, defined for $\epsilon \in [0, \epsilon_0]$ and $\delta \in [-\delta_0, \delta_0]$ (for some sufficiently small $\epsilon_0 > 0$ and $\delta_0 > 0$), along which the vector field (15) has exactly k limit cycles when $\delta \neq 0$*

C			l=1.1	l=1.5	l=3	l=8
	theory box dimension		1/11	1/3	2/3	7/8
0.1	$\mathcal{M}_1$	error estimate	0.056150	0.079995	0.004335	0.110153
		true error	0.056110	0.079903	0.018635	0.580882
	$\mathcal{M}_2$	error estimate	0.051948	0.069960	0.032584	0.003402
		true error	0.051914	0.069900	0.024079	0.160714
	$\mathcal{M}_3$	error estimate	0.064842	0.108443	0.078654	0.032263
		true error	0.064802	0.108371	0.069681	0.009400
0.5	$\mathcal{M}_1$	error estimate	0.031073	0.037178	0.025726	0.121660
		true error	0.031062	0.037161	0.030787	0.568271
	$\mathcal{M}_2$	error estimate	0.028168	0.029094	0	0.011742
		true error	0.028158	0.029082	0.001835	0.160714
	$\mathcal{M}_3$	error estimate	0.038476	0.063678	0.046504	0.019205
		true error	0.038466	0.063664	0.044513	0.004533
1.5	$\mathcal{M}_1$	error estimate	0.018355	0.012709	0.044745	0.129318
		true error	0.018348	0.012701	0.046393	0.559022
	$\mathcal{M}_2$	error estimate	0.016018	0.005647	0.020552	0.021782
		true error	0.016012	0.005642	0.021146	0.160714
	$\mathcal{M}_3$	error estimate	0.025074	0.037994	0.026106	0.010506
		true error	0.025067	0.037988	0.025477	0.000969
6	$\mathcal{M}_1$	error estimate	0.005650	0.013910	0.067191	0.138761
		true error	N/A	0.013915	0.067580	0.546525
	$\mathcal{M}_2$	error estimate	0.003821	0.019937	0.044745	0.034124
		true error	N/A	0.019940	0.044884	0.160714
	$\mathcal{M}_3$	error estimate	0.011667	0.009969	0.001973	0.000232
		true error	N/A	0.009965	0.001833	0.003842

Table 1: Comparison of theoretical error estimates and obtained numerical errors for box dimensions of sequence $x_{n+1} = x_n - F(x_n)$ for $F(x) = Cx^l$. Values (l, C) are from $l \in \{1.1, 1.5, 3, 8\}$ and $C \in \{0.1, 0.5, 1.5, 6\}$. Also, n_0 is fixed at 10^5 and x_0 is fixed at 10^{-2}.

and $\epsilon \in]0, \epsilon_1(\delta)]$ *for some* $\epsilon_1 : [-\delta_0, \delta_0] \to \mathbb{R}$ *with* $\epsilon_1(\delta) > 0$ *for* $\delta \neq 0$. *All these limit cycles are hyperbolic and surround a hyperbolic focus that is attracting when* $\delta < 0$ *and repelling when* $\delta > 0$.

In our fractal approach the starting point is the recursive formula defined in (7):

$$\int_{\alpha(y_n,\delta)}^{\omega(y_{n+1},\delta)} \frac{\left(\frac{\partial H(x,\delta)}{\partial x}\right)^2 dx}{x} = 0, \ n = 0, 1, 2, \dots \tag{16}$$

where the section $\Sigma = \{x = 0\}$ is parametrized by $y > 0$ (see Figure 2), $H(x, \delta) = \frac{1}{2}x^2 + 5\delta x^3 - \frac{35}{46}x^4 - 12\delta x^5 + \frac{21}{46}x^6$, the divergence of (15) for $\epsilon = 0$ is equal to $-\frac{\partial H(x,\delta)}{\partial x}$, the slow dynamics of (15) is given by $x' = -\frac{x}{\frac{\partial H(x,\delta)}{\partial x}} < 0$, $\forall x$, $x = \alpha < 0$, $x = \omega > 0$ and $H(\alpha(y, \delta), \delta) = y = H(\omega(y, \delta), \delta)$. Our goal is to find numerically a small $\tilde{\delta} \neq 0$ and 3 different orbits $U_0^k = \{y_0^k, y_1^k, \dots\}$, $k = 1, 2, 3$, using (16) with $\delta = \tilde{\delta}$, at levels $0 < Y^1 < Y^2 < Y^3$ (i.e. $\lim_{n\to\infty} y_n^k = Y^k$, $k = 1, 2, 3$). The canard cycles Γ_{Y^1}, Γ_{Y^2} and Γ_{Y^3} are balanced (see Section

3). Then we show numerically that $\dim_B U_0^k = 0$, for $k = 1, 2, 3$, and discuss method selection from Section 7.1. See also Theorem 3.3.

7.3.1 Numerical considerations

Formula (16) implicitly defines functions $I_1 = I_1(y, \delta)$ and $I_2 = I_1(y, \delta)$ such that $y_{n+1} = I_1(y_n, \delta)$ and $y_n = I_2(y_{n+1}, \delta)$. There are several considerations to numerical evaluation of I_1 and I_2 for a given y and δ. First, the function $\left(\frac{\partial H(x,\delta)}{\partial x}\right)^2/x$ is a polynomial and can be symbolically computed from function H and for a given δ. The integral in (16) is evaluated using Newton-Leibniz formula and appropriate indefinite integral can be symbolically computed as an integral of a polynomial. Finally, functions α and ω are implicitly given functions and for a given values of y and δ can be numerically computed from $H(\alpha(y, \delta), \delta) = y = H(\omega(y, \delta), \delta)$ using Newtons root finding method. This is implemented using Wolfram Mathematica "FindRoot" function.

For $\tilde{\delta} = 10^{-3}$ we numerically detect three canard cycles at levels Y^k, $k = 1, 2, 3$ (see Table 2). More precisely, by iterating functions I_1 or I_2, from any positive starting value y_0, we either converge to Y^k for some $k = 1, 2, 3$, converge to 0 or diverge to $+\infty$. By iterating for sufficient number of times, starting from above and below Y^k, arbitrary numerical precision for values of Y^k can be achieved.

Canard cycle k	1	2	3
Level Y^k	0.129175	0.194692	1.918008
Orbit length n_0^k	1750	17500	125000
Box dim. using $\mathcal{M}_1$	0.035376	0.046178	0.056111
Box dim. using $\mathcal{M}_2$	0.034496	0.045046	0.054727
Box dim. using $\mathcal{M}_3$	0.038555	0.049315	0.059253

Table 2: Numerically computed box dimensions using method $\mathcal{M}_j$ for the canard cycle at level Y^k with orbit length n_0^k, where $j, k = 1, 2, 3$.

To numerically compute box dimensions of orbits U_0^k, we take $y_0^k := Y^k + 10^{-2}$, $k = 1, 2, 3$. Now we can compute orbits U_0^k to arbitrary length and arbitrary precision. In Table 2 we see numerically computed box dimensions for different methods from Section 7.1 and orbits U_0^k, for a prescribed orbit length n_0^k. The expected theoretical box dimension for every canard cycle k is equal to 0. As already evidenced in Figure 5 and Table 1, in the case of small l the smallest numerical error is achieved using method $\mathcal{M}_2$ (see also Remark 5).

As orbits U_0^k monotonically converge to Y^k and values y_n^k and y_{n+1}^k get closer, we suffer the same problems with loss of numerical precision as described in Section 7.2.2. For our calculations in Table 2 we used precision of 100 decimal places for computing both Y^k and orbits U_0^k, and even more decimal places for internal computations with "FindRoot" function. The computed orbit length n_0^k is limited by precision used. For more details see our Wolfram Mathematica code.

Acknowledgement

This research was supported by Croatian Science Foundation (HRZZ) Grant PZS-2019-02-3055 from "Research Cooperability" program funded by the European Social Fund.

References

[1] E. Benoit. Équations différentielles: relation entrée–sortie. *C. R. Acad. Sci. Paris Sér. I Math.*, 293(5):293–296, 1981.

[2] P. De Maesschalck and M. Desroches. Numerical continuation techniques for planar slow-fast systems. *SIAM J. Appl. Dyn. Syst.*, 12(3):1159–1180, 2013.

[3] P. De Maesschalck and F. Dumortier. Canard cycles in the presence of slow dynamics with singularities. *Proc. Roy. Soc. Edinburgh Sect. A*, 138(2):265–299, 2008.

[4] P. De Maesschalck and F. Dumortier. Classical Liénard equations of degree $n \geq 6$ can have $[\frac{n-1}{2}]+2$ limit cycles. *J. Differential Equations*, 250(4):2162–2176, 2011.

[5] P. De Maesschalck and R. Huzak. Slow divergence integrals in classical Liénard equations near centers. *J. Dynam. Differential Equations*, 27(1):177–185, 2015.

[6] M. Desroches, E. Freire, S. J. Hogan, E. Ponce, and P. Thota. Canards in piecewise-linear systems: explosions and super-explosions. *Proc. R. Soc. Lond. Ser. A Math. Phys. Eng. Sci.*, 469(2154):20120603, 18, 2013.

[7] F. Dumortier. Slow divergence integral and balanced canard solutions. *Qual. Theory Dyn. Syst.*, 10(1):65–85, 2011.

[8] F. Dumortier, D. Panazzolo, and R. Roussarie. More limit cycles than expected in Liénard equations. *Proc. Amer. Math. Soc.*, 135(6):1895–1904 (electronic), 2007.

[9] F. Dumortier and R. Roussarie. Canard cycles and center manifolds. *Mem. Amer. Math. Soc.*, 121(577):x+100, 1996. With an appendix by Li Chengzhi.

[10] F. Dumortier and R. Roussarie. Birth of canard cycles. *Discrete Contin. Dyn. Syst. Ser. S*, 2(4):723–781, 2009.

[11] N. Elezović, V. Županović, and D. Žubrinić. Box dimension of trajectories of some discrete dynamical systems. *Chaos Solitons Fractals*, 34(2):244–252, 2007.

[12] K. Falconer. *Fractal geometry*. John Wiley and Sons, Ltd., Chichester, 1990. Mathematical foundations and applications.

[13] J.-L. Figueras, W. Tucker, and J. Villadelprat. Computer-assisted techniques for the verification of the Chebyshev property of Abelian integrals. *J. Differential Equations*, 254(8):3647–3663, 2013.

[14] P. Grassberger and I. Procaccia. Characterization of strange attractors. *Phys. Rev. Lett.*, 50(5):346–349, 1983.

[15] P. Grassberger and I. Procaccia. Measuring the strangeness of strange attractors. *Phys. D*, 9(1-2):189–208, 1983.

[16] L.-S. Guimond. Homoclinic loop bifurcations on a Möbius band. *Nonlinearity*, 12(1):59–78, 1999.

[17] L. Horvat Dmitrović. Box dimension and bifurcations of one-dimensional discrete dynamical systems. *Discrete Contin. Dyn. Syst.*, 32(4):1287–1307, 2012.

[18] R. Huzak. Box dimension and cyclicity of canard cycles. *Qual. Theory Dyn. Syst.*, 17(2):475–493, 2018.

[19] R. Huzak. Slow divergence integral on a Möbius band. *J. Differential Equations*, 266(10):6179–6203, 2019.

[20] R. Huzak and D. Vlah. Fractal analysis of canard cycles with two breaking parameters and applications. *Commun. Pure Appl. Anal.*, 18(2):959–975, 2019.

[21] M. Krupa and P. Szmolyan. Relaxation oscillation and canard explosion. *J. Differential Equations*, 174(2):312–368, 2001.

[22] C. Kuehn. Scaling of saddle-node bifurcations: degeneracies and rapid quantitative changes. *J. Phys. A*, 42(4):045101, 9, 2009.

[23] C. Kuehn and C. Münch. Duck traps: two-dimensional critical manifolds in planar systems. *Dyn. Syst.*, 34(4):584–612, 2019.

[24] M. L. Lapidus, G. Radunović, and D. Žubrinić. *Fractal zeta functions and fractal drums*. Springer Monographs in Mathematics. Springer, Cham, 2017. Higher-dimensional theory of complex dimensions.

[25] M. L. Lapidus and M. van Frankenhuijsen. *Fractal geometry, complex dimensions and zeta functions*. Springer Monographs in Mathematics. Springer, New York, second edition, 2013. Geometry and spectra of fractal strings.

[26] C. Li and H. Zhu. Canard cycles for predator-prey systems with Holling types of functional response. *J. Differential Equations*, 254(2):879–910, 2013.

[27] J. Llibre, M. Ordóñez, and E. Ponce. On the existence and uniqueness of limit cycles in planar continuous piecewise linear systems without symmetry. *Nonlinear Anal. Real World Appl.*, 14(5):2002–2012, 2013.

[28] P. Mardešić, M. Resman, and V. Županović. Multiplicity of fixed points and growth of ε-neighborhoods of orbits. *J. Differential Equations*, 253(8):2493–2514, 2012.

[29] A. Roberts and P. Gendinning. Canard-like phenomena in piecewise-smooth van der Pol systems. *Chaos*, 24(2):023138, 11, 2014.

[30] H. G. Rotstein, S. Coombes, and A. M. Gheorghe. Canard-like explosion of limit cycles in two-dimensional piecewise-linear models of FitzHugh-Nagumo type. *SIAM J. Appl. Dyn. Syst.*, 11(1):135–180, 2012.

[31] F. Takens. Detecting strange attractors in turbulence. In *Dynamical systems and turbulence, Warwick 1980 (Coventry, 1979/1980)*, volume 898 of *Lecture Notes in Math.*, pages 366–381. Springer, Berlin-New York, 1981.

[32] H. Tong, editor. *Dimension estimation and models*, volume 1 of *Nonlinear Time Series and Chaos*. World Scientific Publishing Co., Inc., River Edge, NJ, 1993.

[33] C. Tricot. *Curves and fractal dimension*. Springer-Verlag, New York, 1995. With a foreword by Michel Mendès France, Translated from the 1993 French original.

[34] C. Tricot. General Hausdorff functions, and the notion of one-sided measure and dimension. *Ark. Mat.*, 48(1):149–176, 2010.

[35] C. Wang and X. Zhang. Canards, heteroclinic and homoclinic orbits for a slow-fast predator-prey model of generalized Holling type III. *J. Differential Equations*, 267(6):3397–3441, 2019.

[36] D. Žubrinić and V. Županović. Poincaré map in fractal analysis of spiral trajectories of planar vector fields. *Bull. Belg. Math. Soc. Simon Stevin*, 15(5, Dynamics in perturbations):947–960, 2008.